■Ngày nhận bài: 15/3/2024 ■Ngày sửa bài: 12/4/2024 ■Ngày chấp nhận đăng: 22/5/2024

Effects of steel slag aggregates on mechanical and electrical resistivity characteristics of high-performance fiber-reinforced concretes

Ảnh hưởng của xỉ thép đến đặc trưng cơ học và điện trở suất của bê tông cường độ cao gia cường cốt sợi

> LE HUY VIET[1,2*], MAI VAN CHUONG[1], NGUYEN SY DUC[1], NGUYEN NGOC HUNG[1], NGUYEN DUY LIEM[3]
[1]Faculty of Civil Engineering, Hanoi University of Mining and Geology
[2]Geotechnical Engineering, Construction Materials and Sustainability Research Group, Hanoi University of Mining and Geology
[3]Faculty of Civil Engineering, Ho Chi Minh City University of Technology and Education.
*Corresponding author: lehuyviet@humg.edu.vn

ABSTRACT

This study investigated the effects of different contents of steel slag aggregates (SSAs) on the mechanical and electrical resistivity properties of high-performance fiber-reinforced concrete (HPFRC). SSAs with a spherical shape and 0.4 mm in maximum diameter were used instead of 0, 30, 50, and 100% content of sand. 2 vol% short smooth steel fibers (0.2 mm in diameter and 13 mm in length) were added to reinforce the high performance concretes with water per cement of 0.2. Two types of steel wire meshes were embedded in samples with a space of 20 mm to measure the electrical resistance of HPFRCs. The test results indicated that the flowability of HPFRC clearly increased from 210 to 270 mm as SSA content (instead of sand) increased from 0 to 100%. The HPFRC with 50% SSA produced the highest compressive strength of 125 MPa. The electrical resistivity of HPFRCs significantly decreased with increasing SSA content. The polarization effect can be ignored after 15 to 20 minutes of direct current measurement for HPFRC matrices with SSAs. In addition, the smaller mesh size of embedded electrodes improved the contacting conduction between electrodes and matrices and decreased the contacting conduction as well as the electrical resistivity of HPFRCs. The microstructure image surrounding fibers was captured and analyzed. A conductive pathway model was proposed based on the microstructure and functional fillers to explain the electrically conductive network in HPFRCs.

Keywords: Electrical resistivity; high-performance concrete; microstructure; smart concrete; steel slag aggregate.

TÓM TẮT

Nghiên cứu đánh giá ảnh hưởng của hàm lượng xỉ thép đến đặc trưng cơ lý và điện trở suất của bê tông cường độ cao gia cường cốt sợi được nghiên cứu. Xỉ thép hình cầu đường kính lớn nhất 0.4 mm được sử dụng thay thế cát với hàm lượng từ 0 tới 100%. Sợi thép mạ đồng với đường kính 0.2 mm, dài 13 mm với hàm lượng chiếm 2% thể tích hỗn hợp được phân tán trong bê tông cường độ cao (tỷ lệ N/X = 0.2). Hai loại lưới thép với kích thước khác nhau sử dụng chôn sẵn vào trong bê tông với khoảng cách 20 mm để làm điện cực đo điện trở của bê tông cường độ cao cốt sợi thép sử dụng dòng điện một chiều (DC). Kết quả nghiên cứu chỉ ra rằng, khi hàm lượng xỉ thép thay thế cát tăng từ 0 đến 100%, độ chảy xòe của HPFRCs tăng từ 210 mm tới 270 mm. Tuy nhiên, cường độ chịu nén của HPFRCs đạt giá trị lớn nhất là 125.2 MPa khi hàm lượng xỉ thép là 50%. Hiện tượng phân cực trong HPFRCs với xỉ thép có thể được bỏ qua sau khi đo điện trở bằng dòng điện một chiều sau 15 đến 20 phút. Điện trở suất của HPFRCs giảm từ 7677.3 tới 4908.7 kΩ-cm khi hàm lượng xỉ thép thay thế cát tăng từ 0 đến 100%. Lưới thép kích thước mắt lưới nhỏ cải thiện khả năng dẫn điện và làm giảm điện trở tiếp xúc giữa lưới thép và bê tông nền. Hình ảnh vi cấu trúc của HPFRCs với xỉ thép được chụp và phân tích. Từ vi cấu trúc của HPFRCs và hàm lượng các chất tăng cường độ dẫn điện (xỉ thép và sợi thép), một mô hình truyền dẫn điện được đưa ra để giải thích đặc trưng về điện trở suất của HPFRCs.

Từ khóa: Bê tông cường độ cao gia cường cốt sợi; bê tông thông minh; điện trở suất; vi cấu trúc; xỉ thép.

1. INTRODUCTION

Sudden collapses of infrastructures without warning caused several people's deaths and enormous economic losses. Some structural catastrophes have recently occurred such as Dhaka Savar Rana Plaza, Bangladesh in 2013 (1134 deaths), Sampoong department store, Korea in 1995 (502 deaths), Hyatt Regency walkway, USA in 1981 (114 deaths), Morandi bridge, Italy in 2018 (43 deaths), Nanfangao bridge, Taiwan in 2019 (6 deaths). Hence, structural health monitoring (SHM) systems have been studied and applied to prevent catastrophic infrastructures. Embedded or attached sensors were generally utilized in the SHM system to detect stress/stress or damage of structures in real time. Figure 1 summarizes some conventional sensors such as Fiber Bragg grating (FBG, Fig. 1a), Lead Zirconate Titanate (PZT, Fig. 1b), and EM sensor (Fig. 1c). However, they have drawbacks such as low durability in comparison to the structure life cycle, high cost, limited sensing area (Han, Yu, and Ou 2014). Besides, embedded sensors (Fig. 1c) would decrease the strength of structures under external loads owing to the generation of weak zones surrounding embedded sensors in the matrix.

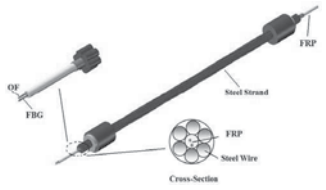

a) Fiber bragg grating (FBG) sensor (Lan C et al. [2012])

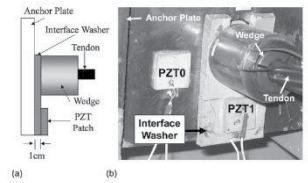

b) Lead Zirconate Titanate (PZT) Sensor (Kim JT et al. [2009])

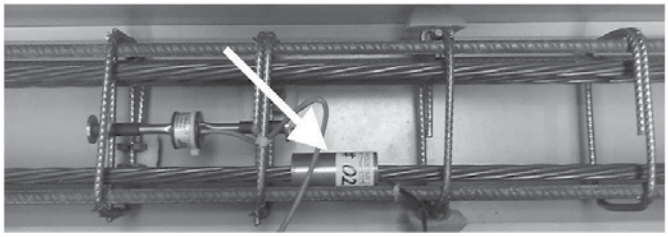

c) Electro-Magnetic (EM) Sensor (Halvonik J et al. [2013])

Figure 1. Some conventional sensors in the SHM system

To overcome the drawbacks of current sensors, smart concrete with self-sensing ability, a new approach, has been developed for application to the SHM system. The stress/strain/damage of smart concretes can be sensed based on their electrical resistivity because of the change in the electrically conductive network under external loads, i.e., the smart concrete becomes a sensor itself. It appeared that the electrical resistivity of smart concrete is a key parameter that significantly influences the self-sensing ability of the smart concrete. Functional fillers with high electrical conductivity such as carbon black, steel fiber, and carbon fibers were generally added to the matrix to enhance the electrically conductive network and the electrical resistivity response of smart concretes under loads (Han et al. 2012; Kim, Kim, and An 2018; Le, Kim, S. U. Kim, et al. 2021; Le and Kim 2017; Viet et al. 2023; Zhang et al. 2020). Thus, the effect of functional filler content should be carefully investigated.

Besides, along with economic development, the need to build high-rise buildings, super high-rise buildings, and large-span bridges is increasing, and materials with high strength and high performance also need to be developed. High-performance fiber reinforced concrete (HPFRC) has been developed and applied to infrastructures owing to great compressive, tensile strengths, high density, and high crack resistance.

This study aims to experimentally investigate the effects of steel slag aggregates, a high electrical conductivity, on the electrical resistivity and the mechanical properties of HPFRCs. The detailed objectives are: 1) to investigate the effects of different contents of SSAs on the mechanical and the electrical resistivity of HPFRCs; 2) to compare It is expected that the study findings will provide useful information for developing and utilizing the self-sensing characteristic of HPFRCs.

2. TYPICAL ELECTRICAL RESISTIVITY BEHAVIOR OF CEMENTITIOUS COMPOSITES

The electrical resistivity (ρ) of the smart concrete is determined based on the electrical resistance (R) measured by using alternative current (AC) (Han, Ding, and Yu 2015; Le, Kim, S. U. Kim, et al. 2021; Lee, Le, and Kim 2019) or direct current (DC) (Le and Kim 2019, 2020; Nguyen et al. 2014; Song and Nguyen 2015) measurements according to Eq. (1).

$$\rho = R\frac{A}{L} \quad (1)$$

where A and L are the cross-section area and the distance between two electrodes in the sample, respectively.

The AC measurement method was preferred to the DC measurement method to obtain the electrical resistivity, which would not be influenced by the polarization and electrode-matrix contacting effects (Han et al. 2014). However, the cost of AC measurement equipment is significantly higher than that of DC measurement. Two and four probes made from highly electrically conductive electrodes such as steel wire mesh, copper wire mesh, copper plate, and copper tape were generally utilized for AC or DC measurements (Han et al. 2015; Le and Kim 2020; Nguyen et al. 2014). Two probes were generally used incorporating AC or DC measurements owing to a simple setup (Han et al. 2014). Thus, in this study, a DC measurement with two probes was utilized to obtain the electrical resistivity of HPFRCs.

Figure 2 shows the typical electrical resistivity of concretes versus time owing to a polarization effect under a DC measurement (Nguyen et al. 2014). As can be seen in Fig. 2, the electrical resistivity significantly changes in the early period but then becomes more stable. Under DC electrical field in direction, the polarization effect was owing to the movement of ions such as K+, Na+, OH–) in continuous pore solution systems (Han et al. 2014). Nguyen et al. indicated that the time of polarization effect of HPFRC was about 20 minutes. The electrical resistivity between electrodes at 20 minutes of DC measurement can be considered as the initial electrical resistivity of concrete and ignore the polarization effect.

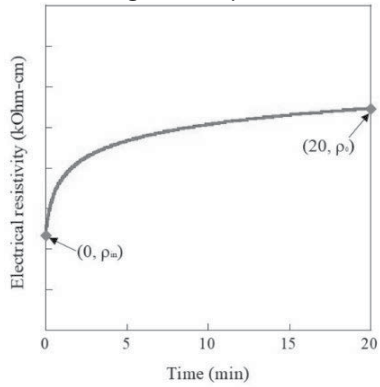

Figure 2. Typical electrical resistivity of concrete with polarization effect (Nguyen et al. 2014)

3. EXPERIMENT

Table 1 summarises the matrix composition of four HPFRCs by

weight ratio. The content of SSAs instead of sand in the F2S0, F2S30, F2S50, and F2S100 matrices was 0, 30, 50, and 100%, respectively. Blended Portland cement (PCB 40) produced by But Son company in Vietnam and silica fume with 90% SiO2 (SF90) were used as binders in the HPFRC matrix composition. Water per cement ratio was 0.2 for all matrices and superplasticizer (SR5000F of Silkroad) was used to enhance the workability of HPFRC matrices. River sand with a diameter lower than 1.25 mm was used. SSAs with a spherical shape and 0.4 mm in maximum diameter were produced by Ecomister, Korea. Figure 3 shows the images of HPFRC matrix compositions. Two types of steel wire meshes (Figure 4a) were embedded in the HPFRC specimens for measuring the electrical resistance.

Specimens were prepared according to steps as follows. Cement, silica fume, river sands and/or SSAs were dry mixed for 5 minutes. Water was gradually poured into the mixture for 2 minutes and then superplasticizer was added and further mixed for 2 minutes. Fresh mixtures were first performed the flow table test using a flow cone. Then, mixtures were poured into cubic specimens (50x50x50 mm^3, Figure 4b). Two steel wire meshes (Figure 4) were embedded into specimens with a space of 20 mm to become electrodes for measuring the electrical resistance. At least three specimens were prepared for each mixture. All specimens were covered by a thin plastic and stored in the laboratory room for 2 days before demolding. Then, they were put into a hot water tank with a controlled temperature of 90°C for 3 days.

Table 1. Matrix composition of HPFRCs by weight ratio

Materials	F2S0	F2S30	F2S50	F2S100_LD	F2S50_MN
Cement	1	1	1	1	1
Silica fume	0.25	0.25	0.25	0.25	0.25
Sand	1.25	0.875	0.625	0	0.625
Water	0.2	0.2	0.2	0.2	0.2
SSA	0	0.375	0.625	1.25	0.625
Superplasticizer	0.05	0.05	0.05	0.05	0.05
Steel fiber	2.0 vol%	2.0 vol%	2.0 vol%	2.0 vol%	2.0 vol%
Electrode type	A	A	A	A	B

a) Cement PCB 40 But Son

b) Silica fume (SF90)

c) River sand

d) SSA

e) Steel fibers

f) Superplasticizer and water

Figure 3. Images of materials in HPFRC matrix compositions

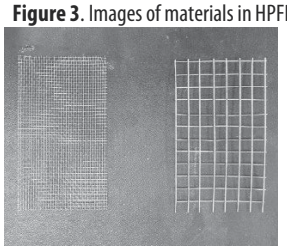

a) Types A (right) and B (left) of electrode

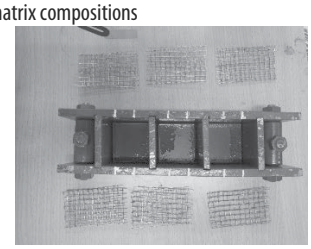

b) Mold (50x50x50 mm^3)

Figure 4. Images of steel wire mesh electrodes and molds

Fig. 5 shows the test setup for measuring the flow value (Fig. 5a), the electrical resistance (Fig. 5b), the compressive strength (Fig. 5c), and scanning electron microscopy (SEM) image capture (Fig. 5d) of HPFRC specimens. ADVANTEST 9 (Controls - Italia) machine with 300 tf capacity was used to determine the compressive strength by maintaining a compressive load of 0.5 MPa/s. The weight of each specimen was measured before compressive testing. The electrical resistance of the HPFRC specimens was measured using the INSTEK GDM 9060 multimeter with two probes. At least three specimens of each HPFRC series were tested to determine the volume weight, electrical resistance, and compressive strength. SEM images were captured using A QUANTA system at the Hanoi University of Mining and Geology.

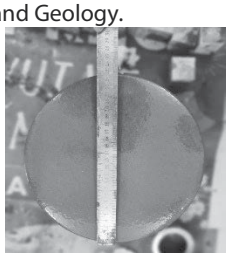

a) Flow table test

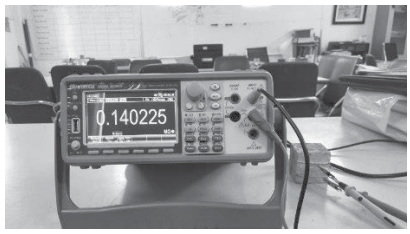

b) Electrical resistance measurement

c) Compressive test

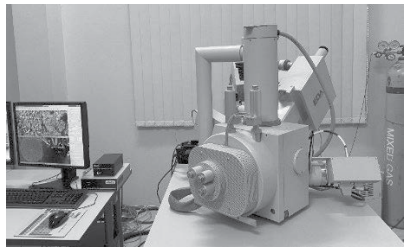

d) SEM image capture

Figure 5. Test setup

4. TEST RESULTS AND DISCUSSION

Figure 6 illustrates the effects of adding SSAs on the workability and compressive strength of HPFRCs. The detailed test results are summarized in Table 2. As the content of SSAs instead of sand increased from 0 to 100%, the flow value of HPFRCs notably increased from 21 to 27 cm while the volume weight increased from 2224 to 3256 kg/m^3. However, the compressive strength of HPFRC increased from 90.8 to 125.2 MPa as SSA content (instead of sand) increased from 0 to 50% then decreased to 104.8 MPa as SSA instead of 100% sand.

Table 2. Flow, volume weight, compressive strength, and electrical resistivity of HPFRCs

Samples		Compressive strength (MPa)	Flow (cm)	Volume weight (kg/m^3)	ρ_{in} (kΩ.cm)	ρ_o (kΩ.cm)
F2S0	SP1	89	21	2208	3665.2	7743.2
	SP2	89.6		2238	3567.2	7683.1
	SP3	94		2228	3698.3	7605.5
	Average	**90.8**		**2224**	**3643.6**	**7677.3**
	STDV	2.2		12,4	55.7	56.4
F2S30	SP1	107.3	22	2416.0	4024.7	6021.5
	SP2	101.4		2480.0	4135.3	6145.3
	SP3	117.8		2416.0	4180.9	6170.6
	Average	**108.8**		**2437.3**	**4113.6**	**6112.5**
	STDV	6.8		30.2	65.6	65.1
F2S50	SP1	123.2	24	2552.0	3475.4	5646.4
	SP2	126.7		2744.0	3760.2	5493.6
	SP3	125.5		2664.0	3556.5	5598.1
	Average	**125.2**		**2653.3**	**3597.4**	**5579.4**
	STDV	1.4		78.7	119.8	63.8
F2S50_MN (wire mesh Type B)	SP1				2143.3	5015.2
	SP2				2206.8	5103.3
	SP3				2215.3	5190.6
	Average				**2188.5**	**5103.0**
	STDV				32.1	71.6
F2S100	SP1	95.8	27	3096.0	1933.2	4910.4
	SP2	108.3		3072.0	2147.2	4935.1
	SP3	110.38		3000.0	2045.3	4880.7
	Average	**104.8**		**3056.0**	**2041.9**	**4908.7**
	STDV	6.4		40.8	87.4	22.2

STDV: standard deviation.

It is clear that the weight of SSAs was significantly higher than that of sand, thus HPFRCs with higher SSA content produced a higher volume weight. In addition, Ecomaister company (www.ecomister.com.) reported that the absorbed water of SSAs was lower 30–40% than that of sands. Zhao et al. 2016 reported that the flowability of concrete was significantly dependent on the free water in the pore solution system. Thus, higher free water in the HPFRC matrices with higher SSA content provided higher flowability. As the SSA content increased from 0 to 50%, higher flowability would enhance the density of the HPFRC matrix and result in higher compressive strength. Besides, sand had higher organic matter which caused weak zones in HPFRC matrices than SSAs and consequently decreased the compressive strength. However, a high flow (270 mm) of F2S100 (100% SSAs instead of sand) would cause segregation of aggregates in fresh mixtures and thus decrease the compressive strength of F2S100 compared to F2S50.

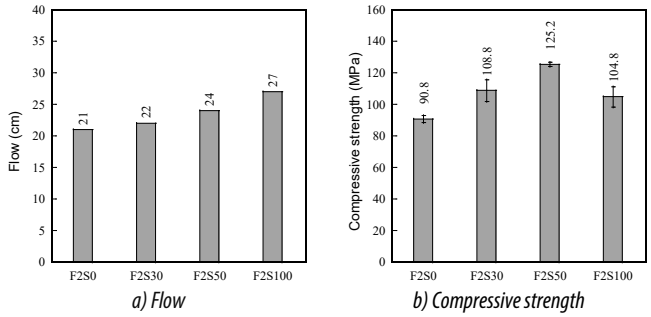

a) Flow *b) Compressive strength*

Figure 6. Effect of SSA content on the flow and compressive strength of HPFRCs

Figure 7 displays the electrical resistivity versus time curves of the HPFRC series: F2S0 (Fig. 7a), F2S30 (Fig. 7b), F2S50 (Fig. 7c), and F2S100 (Fig. 7d), and F2S100_MN. In general, the electrical resistivity significantly changed in the first 5 minutes and then stabilized after 15 to 20 minutes for all HPFRCs with and without SSAs. Nguyen et al. 2014 also obtained a stable electrical resistivity after 20 minutes of DC measurement. Han et al. 2014 indicated that the polarization effect was because of the movement of ions (such as K+, Na+, OH−) in continuous pore systems to electrodes under the DC electric field. Thus, the polarization time was less influenced by the functional fillers in the HPFRCs (steel fibers and SSAs). Hence, to avoid the polarization effect, the change in electrical resistivity owing to external conditions should be considered after 20 min of DC measurement. Table 2 summarizes the average electrical resistivity values and standard deviations of ρ_{in} and ρ_o.

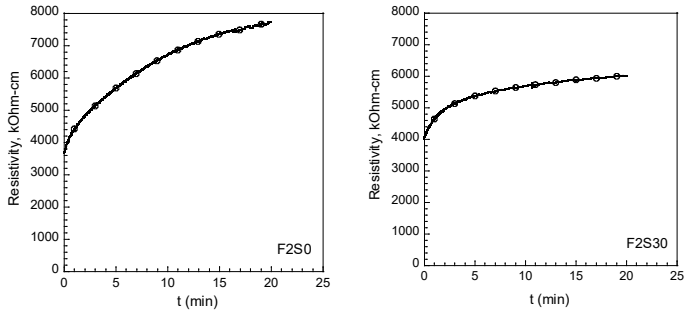

a) F2S0 (SP1) *b) F2S30 (SP1)*

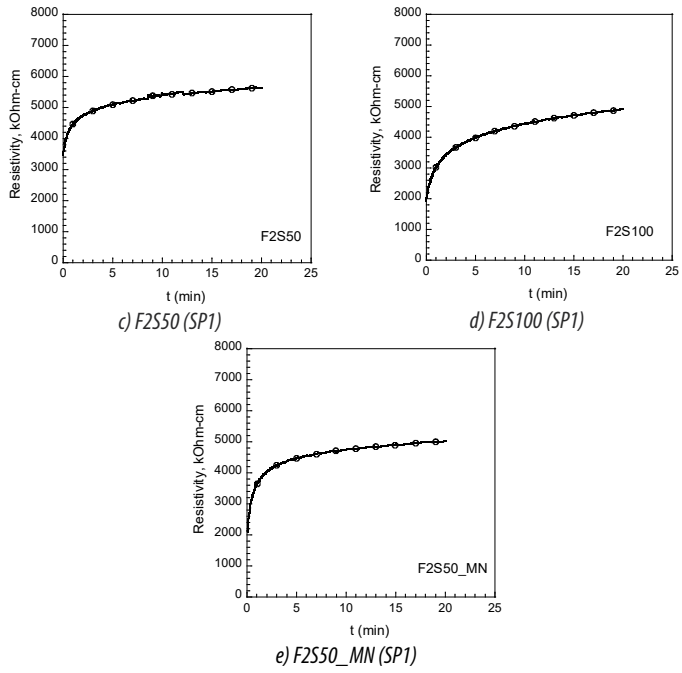

c) F2S50 (SP1) *d) F2S100 (SP1)*

e) F2S50_MN (SP1)

Figure 7. The electrical resistivity versus time of HPFRCs

As shown in Fig. 8, the electrical resistivity (ρ_o) clearly decreased from 7677.3 to 4908.7 kΩ-cm as the SSA content (instead of sand) increased from 0 to 100%. The addition of steel fibers and SSAs increased the contacting and tunneling conductions in the conductive network of HPFRCs (Han et al. 2014). The contacting conduction occurred because of the free electron movement in the contacting functional fillers (steel fibers and SSAs) while the tunneling conduction did because electrons jumped through the energy barriers (matrix) between closed enough functional fillers in a composite (Han et al. 2011; Le, Kim, D. J. Kim, et al. 2021; Song et al. 2015; Yang et al. 2017).

As can be seen in Fig. 8b, the electrical resistivity of samples with wire mesh type A was higher than that of type B. It would be because the smaller mesh size generated a better bond with the matrix, and thus reduced the contacting conduction between electrode and matrix compared to a bigger mesh size.

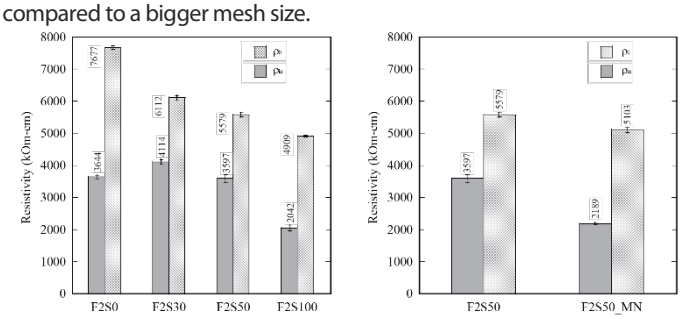

a) Effect of SSA content *b) Effect of electrode types*

Figure 8. Effect of SSA content and electrode types on the electrical resistivity of HPFRCs

As can be seen in Figure 9, the microstructure of the HPFRC matrix was highly denser. There were almost no continuous pores or cracks and few single pores, which resulted in a high compressive strength of HPFRCs in this study (nearly higher than 100 MPa in compressive strength). The addition of silica fume (as an additive and filler material) increased the pozzolanic reaction, filled pores between aggregates, and resulted in a denser microstructure of HPFRCs.

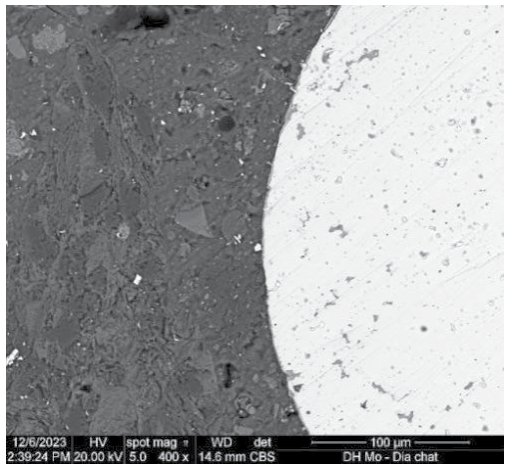

Figure 9. Microstructure image of the matrix surrounding steel fibers (F2S50)

Based on the content of functional fillers and microstructure of HPFRCs, a model of the electrical conductive network in HPFRC matrices was proposed in Figure 10. Conductive paths in the matrix include contacting or tunneling conductions between functional fillers or ionic conduction in a porous solution system. The matrix parts without functional fillers and ionic conduction were considered insulator paths. The conductive network in the HPFRC matrices can be divided into three main pathways: 1) the continuous conductive path (i.e., conductive paths were connected in series); 2) the discontinuous conductive path (i.e., the conductive path connected in series with discontinuous points or insulator point (matrix), and 3) insulator path (the matrix parts without functional fillers or ionic conduction). As the content of SSAs and steel fibers increased, the increasing continuous conductive paths enhanced the electrical conductivity of HPFRCs or decreased their electrical resistivity.

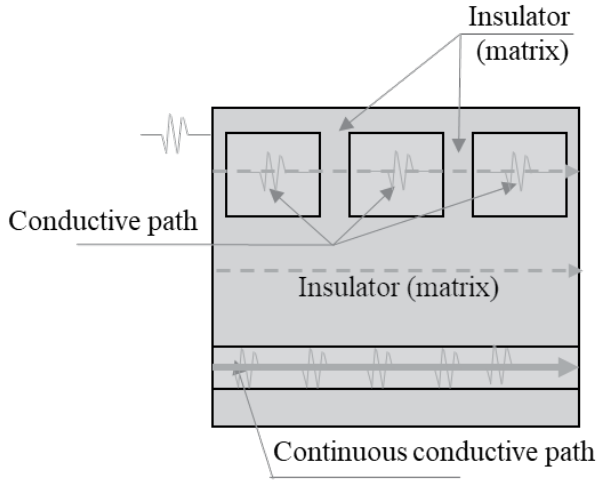

Figure 10. Model of conductive pathways in HPFRCs containing steel fibers and SSAs

5. CONCLUSIONS

The study investigated the effects of adding SSAs on the mechanical and electrical resistivity properties of HPFRCs with short smooth steel fibers. Some conclusions can be drawn as follows:

- The addition of SSAs significantly increased the flowability and volume weight of HPFRCs.
- The HPFRC matrix containing 2 vol% steel fibers and 50% SSAs instead of sand (F2S50) produced the highest compressive

strength (125.2 MPa) in comparison with other HPFRC matrices (F2S0, F2S30, and F2S100).

• The electrical resistivity of HPFRCs notably decreased as the SSAs content increased owing to enhancing the conductive network between functional fillers and/or ionic conduction in the matrix.

• The smaller mesh-size electrodes reduced the contacting resistance between the electrodes and matrix and consequently produced a lower electrical resistivity value of the HPFRC matrix between electrodes.

• The HPFRCs matrix with steel fibers and SSAs had a highly dense microstructure without continuous pores or microcracks.

• A conductive model was illustrated to explain the electrically conductive network as well as the electrical resistivity of HPFRCs containing SSAs.

Acknowledgement:

The authors thank the Hanoi University of Mining and Geology for financial support from Project of Scientific Research potential students in 2022 with the assistance of Dr. Le Huy Viet.

Contributions of authors

Le Huy Viet- methodology, writing draft version, and supervision; Mai Van Chuong, Nguyen Sy Duc, and Nguyen Ngoc Hung - conducting experiments, writing, reviewing, and editing; Nguyen Duy Liem - analyzing data, writing, reviewing, and editing.

REFERENCES

[1]. Han, Baoguo, Siqi Ding, and Xun Yu. 2015. "Intrinsic Self-Sensing Concrete and Structures: A Review." *Measurement* 59:110–28. doi: 10.1016/j.measurement.2014.09.048.

[2]. Han, Baoguo, Xun Yu, and Jinping Ou. 2014. *Self-Sensing Concrete in Smart Structures*. Kidlington: Butterworth Heinemann, Elsevier.

[3]. Han, Baoguo, Kun Zhang, Xun Yu, Eil Kwon, and Jinping Ou. 2011. "Nickel Particle-Based Self-Sensing Pavement for Vehicle Detection." *Measurement* 44(9):1645–50. doi: 10.1016/j.measurement.2011.06.014.

[4]. Han, Baoguo, Kun Zhang, Xun Yu, Eil Kwon, and Jinping Ou. 2012. "Fabrication of Piezoresistive CNT / CNF Cementitious Composites with Superplasticizer as Dispersant." *Journal of Materials in Civil Engineering* (June):658–66. doi: 10.1061/(ASCE)MT.1943-5533.0000435.

[5]. Kim, Min Kyoung, Dong Joo Kim, and Yun Kyu An. 2018. "Electro-Mechanical Self-Sensing Response of Ultra-High-Performance Fiber-Reinforced Concrete in Tension." *Composites Part B: Engineering* 134:254–64. doi: 10.1016/j.compositesb.2017.09.061.

[6]. Le, Huy Viet, and Dong Joo Kim. 2017. "Effect of Matrix Cracking on Electrical Resistivity of High Performance Fiber Reinforced Cementitious Composites in Tension." *Construction and Building Materials* 156:750–60. doi: 10.1016/j.conbuildmat.2017.09.046.

[7]. Le, Huy Viet, and Dong Joo Kim. 2019. "Effects of Matrix Strength, Fiber Type, and Fiber Content on the Electrical Resistivity of Steel-Fiber-Reinforced Cement Composites during Fiber Pullout." *Journal of the Korean Society of Civil Engineers* 39(6):675–89.

[8]. Le, Huy Viet, and Dong Joo Kim. 2020. "Detecting Crack and Damage Location in Self-Sensing Fiber Reinforced Cementitious Composites." *Construction and Building Materials* 240:117973. doi: 10.1016/j.conbuildmat.2019.117973.

[9]. Le, Huy Viet, Min Kyoung Kim, Dong Joo Kim, and Jongwoong Park. 2021. "Electrical Properties of Smart Ultra-High Performance Concrete under Various Temperatures , Humidities , and Age of Concrete." *Cement and Concrete Composites* 118(September 2020):103979. doi: 10.1016/j.cemconcomp.2021.103979.

[10]. Le, Huy Viet, Min Kyoung Kim, Seon Uk Kim, Sang-Yeop Chung, and Dong Joo Kim. 2021. "Enhancing Self-Stress Sensing Ability of Smart Ultra-High Performance Concretes under Compression by Using Nano Functional Fillers." *Journal of Building Engineering* 44(March):102717. doi: 10.1016/j.jobe.2021.102717.

[11]. Lee, Seon Yeol, Huy Viet Le, and Dong Joo Kim. 2019. "Self-Stress Sensing Smart Concrete Containing Fine Steel Slag Aggregates and Steel Fibers under High Compressive Stress." *Construction and Building Materials* 220:149–60. doi: 10.1016/j.conbuildmat.2019.05.197.

[12]. Nguyen, Duy Liem, Jiandong Song, Chatchai Manathamsombat, and Dong Joo Kim. 2014. "Comparative Electromechanical Damage-Sensing Behaviors of Six Strain-Hardening Steel Fiber-Reinforced Cementitious Composites under Direct Tension." *Composites Part B: Engineering* 69:159–68. doi: 10.1016/j.compositesb.2014.09.037.

[13]. Song, J., D. L. Nguyen, C. Manathamsombat, and D. J. Kim. 2015. "Effect of Fiber Volume Content on Electromechanical Behavior of Strain-Hardening Steel-Fiber-Reinforced Cementitious Composites." *Journal of Composite Materials* 49(29):3621–34. doi: 10.1177/0021998314568169.

[14]. Song, Jiandong, and Duy Liem Nguyen. 2015. "Effect of Fiber Volume Content on Electromechanical Behavior of Cementitious Composites." doi: 10.1177/0021998314568169.

[15]. Viet, Le Huy;, Lam; Dao Phuc, Ngo Tri; Thuong, Ngoc Tran; Thanh, Duy Liem; Nguyen, and Dong Joo Kim. 2023. "Improvement of the Stress Sensing Ability of Ultra-High-Performance Concrete Using Short Steel Fibers and Steel Slag Aggregates under High Compression." *Sensors and Actuators: A. Physical* 362(July):114616. doi: 10.1016/j.sna.2023.114616.

[16]. Www.Ecomaister.Com.

[17]. Yang, Haibin, Hongzhi Cui, Waiching Tang, Zongjin Li, Ningxu Han, and Feng Xing. 2017. "A Critical Review on Research Progress of Graphene/Cement Based Composites." *Composites Part A: Applied Science and Manufacturing* 102:273–96. doi: 10.1016/j.compositesa.2017.07.019.

[18]. Zhang, Wei, Qiaofeng Zheng, Ashraf Ashour, and Baoguo Han. 2020. "Self-Healing Cement Concrete Composites for Resilient Infrastructures: A Review." *Composites Part B: Engineering* 189(June 2019):107892. doi: 10.1016/j.compositesb.2020.107892.

[19]. Zhao, Ming, Xiong Zhang, and Yongjuan Zhang. 2016. "Effect of Free Water on the Flowability of Cement Paste with Chemical or Mineral Admixtures." *Construction and Building Materials* 111:571–79. doi: 10.1016/j.conbuildmat.2016.02.057.